



HAL
open science

Impacts of Indo-Pacific sea surface temperature anomalies on the summer monsoon circulation and heavy precipitation over northwest India-Pakistan region during 2010

P. Priya, Milind Mujumdar, T.P. Sabin, Pascal Terray, R. Krishnan

► **To cite this version:**

P. Priya, Milind Mujumdar, T.P. Sabin, Pascal Terray, R. Krishnan. Impacts of Indo-Pacific sea surface temperature anomalies on the summer monsoon circulation and heavy precipitation over northwest India-Pakistan region during 2010. *Journal of Climate*, 2015, 28, pp.3714-3730. 10.1175/JCLI-D-14-00595.1 . hal-01322847

HAL Id: hal-01322847

<https://hal.science/hal-01322847v1>

Submitted on 27 May 2016

HAL is a multi-disciplinary open access archive for the deposit and dissemination of scientific research documents, whether they are published or not. The documents may come from teaching and research institutions in France or abroad, or from public or private research centers.

L'archive ouverte pluridisciplinaire **HAL**, est destinée au dépôt et à la diffusion de documents scientifiques de niveau recherche, publiés ou non, émanant des établissements d'enseignement et de recherche français ou étrangers, des laboratoires publics ou privés.

18

Abstract

19 Quite a few studies have documented the evolution of monsoon synoptic systems and
20 mid-latitude atmospheric blocking associated with the recent heavy precipitation and
21 floods over northwest Pakistan during 2010. This period also witnessed a very unusual
22 Indo-Pacific Sea Surface Temperature (SST) evolution with a strong La Niña event in the
23 Pacific, substantial Indian Ocean warming and a negative Indian Ocean Dipole event,
24 together with significant enhancement of precipitation over both the equatorial western
25 Pacific and the eastern Indian Ocean.

26 Here, we perform a suite of high-resolution Atmospheric General Circulation Model
27 experiments to investigate the influence of Indo-Pacific SST anomalies on the South
28 Asian monsoon circulation and heavy precipitation over Pakistan and adjoining northwest
29 India during 2010. The realistic simulation of these rainfall anomalies using observed
30 SSTs motivated us to explore the specific influence of Indian Ocean and Pacific SST
31 anomalies through additional simulation experiments. Our findings show that, in addition
32 to strengthening of the Pacific Walker circulation, the anomalous intensification of east-
33 west circulation over the Indian Ocean in 2010 was a key element in contributing to
34 precipitation enhancement over the northwest India-Pakistan region. It is found that the
35 subsiding branch of the east-west circulation over Indian Ocean induced anomalous
36 subsidence over the western tropical Indian Ocean and played a key role in inducing
37 northward transport of moisture and promoting generation of strong upward motion and
38 heavy precipitation events over the northwest India-Pakistan region.

39 **1. Introduction**

40 The intense rainfall events over Pakistan during the peak summer monsoon of 2010
41 resulted in the record breaking catastrophic flood in this region, which affected millions
42 of the people (Houze et al. 2011). The humanitarian disaster caused by the July-August
43 2010 flash floods over Pakistan called for a detailed scientific investigation in order to
44 determine if such climate events can be anticipated. The results suggest a potential
45 predictability of about a week based on the ECMWF EPS system (Webster et al. 2011).

46 Since then, many scientific investigations have been conducted to unravel the factors
47 leading to this unprecedented disaster. First, the torrential rainfall over the region is
48 mainly attributed to westward displacement of dramatic weather patterns, which normally
49 occurred over northeastern India and Bangladesh during the monsoon (Houze et al. 2011;
50 Rasmussen et al. 2014). Next, it has been shown that the southward intrusion of mid-
51 latitude weather systems associated with a persistent blocking high over Europe and
52 Russia was one of the key-factors for the occurrence of the northwest India-Pakistan
53 (Indo-Pak) extreme rainfall events (Hong et al. 2011; Lau and Kim 2012; Martius et al.
54 2012; Ullah and Shouting 2013). Hong et al. (2011) suggest that the feedbacks between
55 mid-latitude disturbances downstream of the persistent European blocking high and
56 monsoon surges were the main factors responsible for the extreme rainfall events.

57 However, large-scale patterns of climate variability arising from slowly varying tropical
58 Sea Surface Temperature (SST) boundary conditions are also effective agents for setting
59 up quasi-stationary atmospheric circulation anomalies, which can in turn influence the
60 occurrence of precipitation extremes over smaller regions by modulating synoptic, sub-

61 synoptic and meso-scale variabilities (Trenberth 2012; Yamagata et al. 2004; Behera et al.
62 2013). As an illustration, Behera et al. (2013) have discussed recently the teleconnections
63 of extreme summers in Europe with Indo-Pacific SSTs. In this framework, summer time
64 Indo-Pacific SSTs during 2010 have evolved as the combination of three dominant modes
65 of variability. The year 2010 was marked as one of the strongest La Niña events on long-
66 term record (Mann 2011; Luo et al. 2012;
67 <http://www.bom.gov.au/climate/enso/feature/ENSO-feature.shtml>). Tropical Indian
68 Ocean warming (Kim et al. 2011) and a negative phase of the Indian Ocean Dipole (IOD)
69 phenomenon (Hori et al. 2013) were also prominent during 2010 boreal summer. It is
70 worth mentioning, however, that the 2010 extreme rainfall event over Indo-Pak region is
71 also an unique event in the set of years in which a La Niña and a negative IOD events
72 have simultaneously co-occurred (see Mujumdar et al., 2012).

73 La Niña atmospheric teleconnections generally favor excessive summer monsoon rainfall
74 over south Asia (Rasmussen and Carpenter 1983; Halpert and Ropelewski 1992). It is
75 worth mentioning that some of the past La Niñas (e.g. 1956, 1973 and 1988) also
76 coincided with flood events over the northern Indo-Pak region (Mujumdar et al. 2012).
77 However, among these cold Pacific episodes, 2010 is very unique by the significant
78 westward shift of large-scale circulation over Indo-Pacific sector and the intensification
79 of rainfall activity over northwest India and adjacent sub-tropical Pakistan during boreal
80 summer (Mujumdar et al. 2012). Thus, La Niña induced weakened eastward moisture
81 flux convergence over India and the Bay of Bengal (BoB) was suggested as only a
82 secondary factor responsible for the extreme rainfall events over sub-tropical Indo-Pak
83 region during 2010 (Hong et al. 2011).

84 Similarly, the prominent tropical Indian Ocean warming, which follows the mature phase
85 of the El Niño events, is known to promote abundant rainfall over the Indian subcontinent
86 during the next boreal summer (Yang et al. 2007; Boschat et al. 2011). Some studies have
87 also suggested that anomalous convection associated with positive SST anomalies over
88 the southeast Indian Ocean, as in the 2010 summer, may also promote enhanced rainfall
89 over western India and surrounding areas (Terray et al. 2007). However, the possible
90 roles of Indian Ocean warming during early boreal summer of 2010 or negative IOD
91 event during late summer and fall of 2010 were not explored in the previous studies.

92 Finally, the repeated occurrences of flood episodes over Pakistan and northwest India
93 during 2010, 2011 and 2012 (Rasmussen et al. 2014) question the scientific community
94 about the possible links between these recurrent events and the role of greenhouse
95 warming since extreme events are projected to increase in a warming environment (Chou
96 et al. 2012; Trenberth 2012). Moreover, significant increase of rainfall extremes over
97 India has already been reported in the literature and the role of the sustained Indian
98 Ocean warming trend during recent decades has been suggested (Goswami et al. 2006;
99 Menon et al. 2013; Roxy et al. 2014). But, again the specific role of the global warming
100 environment in promoting the recent flood episodes in the Indo-Pak region is almost
101 unexplored in the previous studies.

102 In other words, the specific role of Indo-Pacific SST anomalies related to El Niño-
103 Southern Oscillation (ENSO), IOD or Indian Ocean warming in the evolution of Indo-
104 Pak extreme rainfall events is not clear from the above studies and is still a matter of
105 debate. Thus, a comprehensive study focusing specifically on the role of SST forcing on
106 the recent Pakistan floods is missing to the best of our knowledge. This prompts us to

107 further investigate these key-questions here in order to improve our understanding of the
108 large-scale SST signals contributing to the occurrence of floods events in the Indo-Pak
109 region. Since observations alone are not sufficient to delineate quantitatively the role of
110 the different SST signals on the Pakistan flood of 2010, these questions are tackled in a
111 modeling framework with a help of various sensitivity experiments conducted with an
112 Atmospheric General Circulation Model (AGCM). More precisely, various sets of
113 ensemble simulation experiments with a high resolution AGCM were carried out to
114 understand the contributions of various aspects of Indo-Pacific SST forcing in triggering
115 the extreme summer monsoon rainfall activity over sub-tropical South Asia.

116 The paper is organized as follows. A description of the AGCM, the precise setup of our
117 various sensitivity experiments, the observed datasets and statistical tools used in our
118 diagnostic analysis is provided in Section 2. Section 3 assesses the realism of simulations
119 of large-scale circulation patterns over Indo-Pacific region associated with sub-tropical
120 South Asian extreme rainfall events from a set of simulations forced with observed SST
121 anomalies during 2010. Section 4 is devoted to a quantitative assessment of the role
122 ENSO and ENSO-unrelated SST anomalies on the 2010 flood events with the help of
123 several dedicated sets of sensitivity experiments conducted with the same AGCM.
124 Analysis of the divergent and non-divergent components of the anomalous vertically
125 integrated water vapor transport in the sensitivity experiments is provided in Section 5 in
126 order to unravel the role of intrinsic Indian Ocean variability during 2010. The discussion
127 and summary are presented in the last section.

128 **2. Datasets, methods, SST boundary forcings and numerical experiments**

129 Our diagnostic and simulation analyses are mostly focused on summer monsoon season
130 (June-September, JJAS hereafter) of 2010. For a comparison of rainfall between
131 observations and the model outputs, we used gridded rainfall data ($0.25^\circ \times 0.25^\circ$) from
132 Tropical Rainfall Measuring Mission (TRMM), specifically the 3B42-V6 product from
133 1998 to 2010 (Huffman et al. 2007). Mean sea level pressure and atmospheric circulation
134 at standard pressure levels are taken from National Center for Environmental Prediction
135 and National Center for Atmospheric Research (NCEP/NCAR) reanalysis (Kistler et al.
136 2001). The SST data are based on the Hadley Centre Sea Ice and Sea Surface
137 Temperature (HadISST) dataset (Rayner et al. 2003).

138 The evolution of SST monthly anomalies for the period January to September 2010 is
139 shown in Figure 1 along with seasonal (JJAS) SST anomalies. As illustrated by Fig. 1a,
140 2010 is marked by a very unusual Indo-Pacific SST evolution with a very fast transition
141 from a warm pool El Niño during 2009 to a strong La Niña event in the equatorial Pacific
142 a few months later. Interestingly, this rapid transition was accompanied by a prominent
143 warming of the tropical Indian Ocean during spring and early summer of 2010. Kim et al.
144 (2011) have illustrated the dominant contribution of the basin-wide Indian Ocean
145 warming in the fast evolution of the 2010 La Niña from the preceding El Niño episode.
146 When the Indian Ocean is warm, the induced anomalous easterlies over the west and
147 central equatorial Pacific can trigger an upwelling thermocline anomaly propagating
148 eastward that fastens the transition from El Niño to La Niña (Kug and Kang 2006).

149 In order to delineate quantitatively the relative role of ENSO and other factors (e.g.
150 global warming or intrinsic Indian Ocean variability) in the Indo-Pacific SST evolution
151 during 2010, the linear inverse modeling approach of Compo and Sardeshmukh (2010)

152 was used. This approach is one of the best methods currently available to isolate ENSO
153 component in climate time series as demonstrated by the work of Penland and coworkers
154 during the last two decades (see
155 <http://www.esrl.noaa.gov/psd/people/cecile.penland/pubs.html>). The ENSO and ENSO-
156 unrelated components of monthly SST anomalies during 2010 were kindly provided by
157 Dr. Compo through personal communication. These components for 2010 were estimated
158 using exactly the same technique as described in Compo and Sardeshmukh (2010) and
159 are displayed in Figs. 1b and c, respectively. Here, it should be noted that ENSO-
160 unrelated SST anomalies represent the combination of anthropogenic forced and
161 internally coherent multi-decadal to interannual SST variations not related to ENSO
162 (Compo and Sardeshmukh 2010). The anomalous cooling over north subtropical and
163 eastern equatorial Pacific observed in the ENSO component, as soon as March 2010,
164 significantly marks the fast transition to a La Niña state (Fig. 1b). However, the Pacific
165 SST anomalies observed during 2010 are also strongly modulated by the ENSO-unrelated
166 component with anomalous warming (cooling) over western and eastern equatorial
167 (north-west and central) Pacific regions.

168 The prominent warming over tropical Indian Ocean is consistent throughout the season,
169 though it is weaker in September. It is noteworthy, that the basin-wide Indian Ocean
170 warming during 2010 is mostly attributed to ENSO (since the ENSO-unrelated
171 component mostly promotes cooling in the central Indian Ocean during 2010), but with
172 two important exceptions in the northwest Arabian Sea and the southeast Indian Ocean,
173 respectively. These two regions witnessed warm SST anomalies from March onward in
174 the ENSO-unrelated component during 2010. The northwest Arabian Sea warming is

175 particularly significant (Fig. 1a) and is mostly contributed by the ENSO-unrelated
176 variability (Fig. 1c). Similarly, the SST pattern associated with the 2010 negative IOD
177 event (with positive SST anomalies over the southeast Indian Ocean and negative
178 anomalies further west) is already seen from June onward in the ENSO-unrelated
179 component (Hori et al. 2013).

180 In summary, observed SSTs during 2010 include all types of SST components mentioned
181 above. Thus, in order to further delineate the impacts of these various SST boundary
182 forcings on the 2010 monsoon, we have performed a suite of 5 ensemble sets of seasonal
183 (May-October) simulation experiments using a high resolution AGCM. The model used
184 is a state-of-the-art global model (LMDZ4; Z stands for zoom) developed at the
185 Laboratoire de Météorologie Dynamique (France). The model has been zoomed to ~ 35
186 km x 35 km over the Indian Summer Monsoon (0 – 40°N, 45°E – 110°E) region (Sabin et
187 al. 2013). The time varying forcing agents in the AGCM, e.g. atmospheric CO₂, CH₄,
188 N₂O etc., are set to present values. Other details of the AGCM are provided by Hourdin et
189 al. (2006) and Sabin et al. (2013), and are not repeated here for conciseness.

190 The five ensemble sets of experiments differ from each other only with regards to the
191 specification of the SST boundary conditions. Each of these sets comprises of ten
192 simulations starting from the 16th May 2010. Ten perturbed initial conditions for these 10
193 realizations were generated following a slight variation of the method described in Sabin
194 et al. (2013). Starting from initial conditions based on the ECMWF analysis for the
195 month of January, ten 2-year simulations forced with repeated observed SSTs for each
196 year of the 2000-2009 period were first performed with the AGCM. Model dumps were
197 stored for every 15th day intervals and the 10 model dumps for 16th May of the second

198 year constitute the 10 perturbed initial conditions.

199 The details and acronyms of the five sets of experiments performed are summarized in
200 Table 1. The first set of experiments, labeled as C-SST, uses climatological SSTs as
201 boundary conditions. The large-scale, as well as the regional, features of the South Asian
202 summer monsoon are realistically simulated by the C-SST control runs, thanks to the
203 telescopic zoom over the Indian domain (Fig. 2). The strong moisture advection from
204 Arabian Sea and BoB into the Monsoon Trough zone is also well captured by the C-SST
205 runs (Fig. 2b). The wide spread rainfall distribution over Indian subcontinent in LMDZ
206 simulations is seen to be closely associated with strong south-westerly flow over Arabian
207 Sea as observed. The large-scale cyclonic circulation associated with the Monsoon
208 Trough, the significant strengthening of near equatorial convection and cross-equatorial
209 flow are also well captured, in addition to the synoptic features associated with the
210 monsoon (see Sabin et al. 2013). However, the difference of observed rainfall
211 climatology with that of C-SST shows a wet bias over the South Asian Monsoon domain
212 and the Maritime Continent (Fig. 2c). These biases are associated with stronger easterlies
213 over Maritime continent and a, strong moisture advection from Arabian Sea and BoB to
214 the Indian subcontinent, respectively. Interestingly, the simulated rainfall over the
215 Monsoon Trough region (covering north-central India), narrow mountain range of
216 Western Ghats and Myanmar is more realistic than in the standard version of the LMD
217 model (Sabin et al. 2013). The realism of the monsoon (due to the use of high-resolution
218 zooming) in the C-SST experiments suggests that the LMDZ model is an interesting tool
219 for studying the role of different SST forcings in the 2010 monsoon with the help of
220 sensitivity experiments.

221 The second experiment (R-SST) uses observed SSTs of 2010. The significant
222 modulations of the Indo-Pacific SST patterns during 2010 by the ENSO-unrelated
223 component are particularly intriguing and warrant further investigation with respect to the
224 occurrence of the heavy precipitation events during 2010. Thus, the next two sets of
225 ensemble experiments are carried out by using, respectively, ENSO and ENSO-unrelated
226 SST anomalies (see Figs. 1b and c) superimposed on the monthly climatological SST
227 (computed from the period 1948-2010) as boundary forcing conditions for 2010. These
228 third and fourth ensemble sets are labeled E-SST and NE-SST, respectively (Table 1).
229 Finally, the significant contribution from intrinsic Indian Ocean variability during 2010 is
230 brought out by conducting a fifth ensemble of sensitivity experiments retaining ENSO-
231 unrelated SST anomalies over Indian Ocean (40-110°E and 15°S-28°N) and
232 climatological SST elsewhere. Thus, in this last set of experiments, labeled as NE-IO-
233 SST, both the Pacific SST interannual variability and the ENSO-related signal in the
234 Indian Ocean are suppressed.

235 The synoptic scale convective activity associated with low-level moisture convergence
236 and extreme rainfall events can be better understood by the analysis of daily minimum
237 mid-tropospheric (500 hPa) vertical wind velocity (Hourdin et al. 2006). In the present
238 study we employ Weibull distribution fitting, as a guiding and descriptive tool, to
239 understand how daily mid-tropospheric vertical velocity is varying over the northwest
240 Pakistan region (70°–74°N; 30°–36°E) during summer of 2010 in the different sets of
241 simulation experiments. The Weibull distribution is a special type of extreme value
242 distribution, which has been extensively used to study the behavior of the lower tail of a
243 data sample distribution and to model wind speed statistics (Conradsen et al. 1984, Sarkar

244 et al. 2011). First, the time series of daily minimum values of 500 hPa vertical wind
245 velocity (e.g. omega at 500 hPa) over the northwest Pakistan region during JJAS of 2010
246 is extracted from each of the ten members of a given set of experiments in Table 1.
247 Secondly, these concatenated time series are considered as the sample of daily extremes
248 for this particular set of experiments. As an illustration, the sample of daily minimum
249 values of 500 hPa vertical wind velocity for the C-SST set contains 1220 time steps (122
250 days by 10 members). Finally, the two parameters (e.g. the shape and scale parameters) of
251 the Weibull distribution (Rousu 1977; Justus et al. 1978) are estimated from this sample
252 by using the maximum likelihood method at 95% confidence level (Bowden et al. 1983).
253 As an illustration, we show in Figure 2d, the histogram of these extreme values in the C-
254 SST runs overlaid by the Weibull Probability Density Function (PDF) fitted to this
255 particular sample of daily minimum values of 500-hPa vertical wind velocity. The
256 Weibull distribution fits well the form of the histogram due to its flexibility with two
257 estimated parameters (e.g. shape and scale parameters). This demonstrates the usefulness
258 of Weibull distribution fitting to model extreme daily upward velocity over northwest
259 Pakistan during 2010 and to better describe synoptic scale convective activity in our
260 different sets of experiments.

261 **3. AGCM experiments with observed SSTs**

262 The spatial distributions of rainfall and vertically integrated moisture transport anomalies
263 during the 2010 boreal summer (JJAS) in observations and the R-SST simulations are
264 displayed in Figure 3. The observed enhanced summer monsoon rainfall over northwest
265 Indo-Pak region, equatorial west Pacific and eastern Indian Ocean is well simulated by
266 the R-SST runs. The spatial correlation between the observed and simulated boreal

267 summer rainfall anomalies (in the R-SST experiments) is as high as 0.45 for the domain
268 50°-110°E and 15°S-40°N, and increased to 0.49 if the domain is extended farther east,
269 up to 120°E. These correlations are significant at the 95% confidence level according to a
270 Student t-test. This suggests that the SST boundary conditions play a significant role in
271 setting up the background atmospheric state associated with the heavy rainfall event over
272 Pakistan during the 2010 boreal summer. The reduced amplitude of the rainfall anomalies
273 over the northwest Indo-Pak region in the R-SST runs (Fig. 3b) may be due to the
274 improper representation of mid-latitude blocking during boreal summer of 2010 by the
275 model (figure not shown). The anomalously weaker monsoon rainfall activity over
276 central and eastern India, BoB and adjoining areas of the South China Sea and Philippine
277 Sea is also less pronounced in R-SST runs than in observations (Figs. 3a and b).
278 However, important key features such as anomalous northward moisture transport in the
279 Arabian Sea and Indo-Pak regions, westward penetration of anomalous easterlies over the
280 south-eastern Indian Ocean, strong anomalous cyclonic circulation over the southeast
281 Indian Ocean and Indo-Pak regions are well captured.

282 The Weibull distribution diagnostic described in Section 2 has been applied to the
283 minimum daily mid-tropospheric (500 hPa) vertical velocity time series extracted from
284 the northwest Pakistan region in the C-SST and R-SST runs (Fig. 4). First, as expected,
285 we note that the R-SST simulations failed to reproduce the exact timing of the heavy
286 rainfall events over the northwest Pakistan since the simulations were start from the 16th
287 May from random initial conditions. However, the significant contribution from SST
288 anomalies to daily synoptic scale convective activity over northwest Pakistan region
289 during 2010 is well brought out by the elongated tail of the Weibull distribution for the R-

290 SST simulations, which is the characteristic of a high probability of extreme convective
291 activity at daily time scale during 2010. On the other hand, the tail of the Weibull
292 distribution in case of the C-SST simulations is much shorter with no values below -2.2
293 hPa/s (Fig. 4).

294 Focusing now on the tridimensional atmospheric circulation during 2010, the
295 anomalously enhanced convection over north Arabian Sea and northwest Pakistan region
296 (Fig. 3a) is associated with strong upward vertical velocity anomalies from low levels up
297 to the tropopause level and seems to descend south of the equator (Fig. 5a). This
298 anomalous meridional structure over the western part of the Indian domain is reasonably
299 captured by the R-SST runs, though the sinking motion is slightly more to the south in
300 model compared to observations (Fig. 5b). The positive SST anomalies over the southeast
301 Indian Ocean associated with La Niña and the growing phase of negative IOD event
302 (Figs. 1b and c) promote abundant local rainfall in both observations and R-SST runs
303 (Figs. 3a and b). Interestingly, the upper level outflow associated with these strong
304 convection anomalies over the Maritime continent and southeast Indian Ocean may also
305 induce a strong modulation of the Indo-Pacific Walker circulation and local meridional
306 cell in the eastern part of the Indian region in observations (Figs. 5c and e). It is
307 noteworthy that the R-SST experiments simulate realistically the large-scale subsidence
308 over north BoB and eastern India, on one hand, and over central and western Indian
309 Ocean (to the west of the 80°E), on the other hand, which may be induced by the
310 ascending branch over the southeast Indian Ocean (Figs. 5d and f). The large-scale
311 subsidence over the Indian Ocean (to the west of 80°E and south of the equator) and the
312 strong northward moisture transport over north Arabian Sea and Indo-Pak region are

313 consistent in both observations and the R-SST runs, amidst the weaker southwesterly
314 flow in the simulations (Fig. 3b). This result is consistent with the findings of Mujumdar
315 et al. (2012). Thus, despite of the fact that the R-SST simulations do not reproduce the
316 observed mid-latitude blocking during boreal summer of 2010, the observed seasonal
317 rainfall and circulation anomalies, as well as the intense convective activity over
318 northwest Pakistan are surprisingly reasonably captured.

319 In order to highlight the key physical processes involved in the anomalous rainfall
320 distribution during 2010 and delineate the role of the various SST forcings (Figs. 1b and
321 c), we will focus on the sensitivity experiments in the two following sections.

322 **4. Sensitivity experiments with ENSO and ENSO-unrelated related SST** 323 **anomalies**

324 The realistic simulation of sub-tropical rainfall anomalies over the Indo-Pak region and
325 observed atmospheric circulation during 2010 by the R-SST runs further motivates us to
326 distinguish the roles of ENSO and ENSO-unrelated SST patterns in promoting the Indo-
327 Pak rainfall events with the help of the E-SST and NE-SST runs (see Table 1).

328 The possible role of the 2010 La Niña event in promoting Indo-Pak flood event was
329 already suggested in previous studies (Hong et al. 2011; Mujumdar et al. 2012). As
330 expected, the E-SST experiments simulate a prominent response over the tropical Pacific,
331 such as a stronger east (suppressed) – west (enhanced) equatorial rainfall gradient,
332 vigorous trade winds and enhanced convection over northwest Pacific (Fig. 6a).
333 Similarly, E-SST runs reproduce the observed anomalous easterly flow over central India,
334 weakening of the Monsoon Trough and associated decreased monsoon rainfall over North

335 India. However, E-SST experiments fail to reproduce enhanced rainfall over Indo-Pak
336 region at the seasonal time scale (Fig. 6a). In agreement with this result, the spatial
337 correlation between the observed and simulated seasonal rainfall anomalies by E-SST
338 runs is drastically decreased (e.g. 0.19) compared to R-SST experiments (domain used is
339 again 50°-110°E and 15°S-40°N).

340 Furthermore, Weibull distribution analysis is repeated here to understand how the
341 extreme synoptic scale convective activity over northwest Pakistan varies in the
342 sensitivity experiments. The number of days with enhanced convective activity over the
343 region is significantly decreased in E-SST runs compared to R-SST set of experiments
344 (Fig. 4). The left tail of the Weibull distribution in the E-SST runs is even shorter than the
345 one in the C-SST runs. Furthermore, the frequency count of extreme rain events over the
346 northwest Pakistan region (e.g. greater than 95th percentile estimated from the C-SST
347 daily rainfall values) is almost 3 times higher in R-SST runs compared to those of E-SST
348 runs. These statistical analyses using rainfall and vertical velocity bring out the
349 significant difference in extreme rainfall events in R-SST and E-SST runs, and
350 demonstrate that the ENSO SST forcing alone is not sufficient to promote extreme
351 convective activity over northwest Pakistan. These disagreements between the E-SST and
352 R-SST experiments are intriguing. It is therefore interesting to investigate the influence of
353 the ENSO-unrelated SST patterns on subtropical Indo-Pak heavy rainfall with the help of
354 the NE-SST and NE-IO-SST ensemble simulation experiments (see Table 1).

355 The observed suppressed rainfall associated with stronger anomalous easterly wind
356 induced moisture divergence over north India are not well reproduced by the NE-SST and
357 NE-IO-SST runs, especially for NE-SST set (Figs. 6b and c). These observed features are

358 clearly due to the ENSO component to first order (Fig. 6a). Interestingly, the observed
359 rainfall and moisture transport anomalies over Arabian Sea are reasonably captured by
360 the NE-SST, NE-IO-SST experiments (Figs. 6b and c), while the E-SST runs fail to
361 simulate these regional anomalies (Fig. 6a). Similarly, enhanced convection over south-
362 east Indian Ocean and suppressed convection over central Indian Ocean, and BoB are
363 well captured in the NE-SST and NE-IO-SST runs (Figs. 6b and c). Due to these
364 similarities, the spatial correlations of observed rainfall anomalies with the simulated
365 rainfall anomalous patterns in the NE-SST and NE-IO-SST experiments are 0.22 and
366 0.27, respectively. These scores are higher than the one obtained from the E-SST
367 experiments (e.g. 0.19), which fails to capture the subsidence over central and western
368 Indian Ocean.

369 Furthermore, the key influence of Indian Ocean SST anomalies unrelated to ENSO in
370 promoting the occurrence of extreme rainfall events over northwest Pakistan is also
371 illustrated by the Weibull diagnostic applied to the NE-SST and NE-IO-SST runs (Fig. 4).
372 The interesting feature of the probability density curve in case of NE-SST and NE-IO-
373 SST experiments is its elongated tail compared to the E-SST runs, tending to the one
374 found in the R-SST runs, which indicates a higher probability of extreme daily upward
375 motion over the northwest Pakistan region, evolving from deep convection induced by
376 lower level moisture convergence (Fig. 4). This elongated tail, which characterizes the
377 occurrence of intense convective activity at the daily time scale, is highlighted in the inset
378 of the Fig. 4. We have also confirmed that total count of extreme rainy days during
379 monsoon season is generally higher in NE-SST and NE-IO-SST runs relative to C-SST
380 and E-SST ensembles (figure not shown).

381 All these results bring out the key role of ENSO-unrelated SST anomalies and, in
382 particular, highlight the significant influence of intrinsic Indian Ocean variability in the
383 amplification and sustenance of extreme rainfall events over the subtropical Indo-Pak
384 region. The next section investigates the physical mechanisms explaining the key role of
385 ENSO-unrelated SST anomalies over Indian Ocean on the northward moisture transport
386 over Arabian Sea during 2010.

387 **5. Mechanisms for moisture convergence over the northwest Pakistan during**
388 **2010.**

389 Here an attempt is made to understand how various SST boundary forcings may have
390 contributed to the anomalous moisture transport over northwest Pakistan and promoted
391 heavy rainfall events of 2010. In particular, it would be worth analyzing the role of the
392 zonal asymmetry of convection over equatorial Indian Ocean (Fig. 3a) in modulating
393 northward moisture transport over Arabian Sea and northwest Pakistan region. For this
394 purpose, stream and potential functions of vertically integrated (from surface to 300 hPa)
395 moisture flux anomalies were decomposed into irrotational and rotational components, in
396 the different sets of simulations (Chen 1985; Krishnan 1998). These functions provide a
397 concise description of spatial distributions of moisture convergence and moisture
398 transport, respectively, for 2010 boreal summer in simulation experiments.

399 We first try to get a better understanding of the physical mechanism responsible for the
400 local maintenance of high water vapor content over northwest Pakistan during 2010 by
401 using the potential of integrated moisture transport anomalies and its divergent
402 component in R-SST, E-SST and NE-SST sets of simulations (Fig. 7). The statistically

403 significant regions at the 95% confidence level are marked in these figures. Since the
404 results for NE-SST and NE-IO-SST ensembles are very similar, here we discuss NE-SST
405 results only. The divergent component of vertically integrated moisture flux in R-SST
406 and E-SST simulations are very similar and exhibit a strong moisture convergence over
407 Indian Ocean and Maritime Continent and large-scale moisture divergence over Central
408 Pacific (Figs. 7a and b). On the other hand, NE-SST simulations suggest that the moisture
409 converges, primarily, towards southeast Indian Ocean and Maritime continent and,
410 secondarily, toward north Arabian Sea and northwest Pakistan areas (Fig. 7c). This
411 suggests that the zonal component of divergent moisture transport during 2010 is mostly
412 accounted by the modulation of Walker circulation and the westward shift of zonal
413 circulation associated with the strong La Niña event and the related Indian Ocean
414 warming (Fig. 8d). Interestingly, the southeast-northwest tilted orientation of the region
415 of anomalous moisture convergence over the Indian domain in the R-SST simulations
416 (Fig. 7a) seems to be mostly maintained by ENSO-unrelated SST variability over the
417 Indian Ocean. Hence this SST pattern may have contributed to the modulation of the
418 local meridional and zonal circulations over Indian Ocean (Figs. 8a and c). More
419 specifically, the enhanced convection over south-eastern Indian Ocean (Fig. 3a)
420 associated with the growing phase of negative IOD event (Figs. 1c, 6b and 6c) is well
421 marked by anomalous moisture convergence, which is statistically significant at the 95%
422 confidence level in NE-SST runs (Fig. 7c). This region of intense convection extends
423 eastward over the Maritime Continent, while its western counterpart, the region of
424 suppressed convection over the western and central Indian Ocean (see Figs. 3a and 6b, c),
425 coincides with a region of moisture divergence (Fig. 7c). In other words, the zonal

426 gradient of SST over the Indian Ocean in the NE-SST runs seems to induce moisture
427 convergence and ascending motion over southeastern Indian Ocean and, in turn, moisture
428 divergence and descent over western and central equatorial Indian Ocean (Fig. 8c; see
429 Lindzen and Nigam, 1987).

430 It is also interesting to note that the conventional region of moisture divergence over
431 central Arabian Sea (Saha and Bavedekar 1973; Rao and Van de Boogard 1981 and Cadet
432 and Reverdin 1981) is dominated by significant moisture convergence during the 2010
433 summer in NE-SST simulations. This helps to maintain the tilted configuration of the
434 potential fields over the Indian domain in the R-SST simulations (Figs. 7a and c). The
435 positive meridional SST gradient between north Arabian Sea [60° - 70° E, 15° - 25° N] and
436 western equatorial Indian Ocean [55° - 70° E, 5° S- 7° N] (see Fig. 1c), together with the
437 moisture divergence over equatorial Indian Ocean (Fig. 7c), might have contributed to the
438 enhanced moisture convergence over north Arabian Sea in NE-SST runs (Fig. 6c).
439 Upward motion overlies this region of moisture convergence and enhanced rainfall (over
440 north Arabian Sea and adjacent areas), while subsidence coincides with the region of
441 moisture divergence in NE-SST runs (Fig. 8a). On the other hand, E-SST runs depict a
442 strong ascent over equatorial Indian Ocean with a descent over northwest Pakistan region
443 (Fig. 8b), which is significantly different from R-SST experiment (Fig. 5b). These results
444 further highlight the important role of intrinsic Indian Ocean SST anomalies on
445 northward moisture transport over Arabian Sea through the modulation of convergent and
446 divergent zones by the SST gradients in NE-SST runs.

447 The stream function and the rotational component of the integrated moisture flux
448 anomalies may be used to illustrate how the water vapor transport is maintained in the

449 simulations (Fig. 9). It is apparent that the large-scale patterns of stream function and
450 rotational component of moisture transport during 2010 are largely contributed by the
451 ENSO-related SST anomalies, as demonstrated by the strong similarities between the
452 potential fields in the R-SST and E-SST sets of simulations (e.g. compare Figs. 9a, b and
453 c). In particular, the strong and large-scale southeast-northwest orientation of stream
454 function over the Indo-Pacific domain displayed in Figs. 9a and b reflects a strong
455 anticyclonic structure over BoB and central India, resulting in suppressed convection
456 over the region (Fig. 1b), which seems to be induced by the ENSO-related SST
457 anomalies, This is in agreement with the result of Mujumdar et al. (2012). At the same
458 time, R-SST and E-SST runs depict an anomalous southeasterly moisture transport over
459 northwest Pakistan region, which is consistent with the results of Hong et al. (2011).
460 However, E-SST experiment failed to capture enhanced rainfall activity over the
461 northwest Pakistan region (Fig 6a).

462 On the other hand, the stream function and rotational component computed from
463 moisture flux anomalies in NE-SST experiments exhibit a four-cell structure over the
464 Indian domain. It is evident from the comparison between Figs. 9a, b and c that this
465 cellular pattern of stream function in NE-SST simulation, which is related to intrinsic
466 Indian Ocean variability, is significantly weaker in intensity compared to the moisture
467 transport induced by the ENSO-related SST variability and that the large-scale features of
468 the stream function in the R-SST and E-SST simulations are very similar. However, the
469 strengthening of anomalous anticyclonic circulation over central India and Arabian Sea in
470 the NE-SST runs is remarkable (Fig. 9c). This phenomenon intensifies the northwestward
471 shift of anomalous moisture transport over Indo-Pacific sector prevailing during the La

472 Niña episode of 2010 (Figs. 9a and c). Furthermore, the southwesterly flank of this
473 anomalous anticyclonic circulation (Fig. 9c), together with the regional divergent
474 component of moisture flux (Fig. 7c), seems to promote strong northward moisture
475 transport over Arabian Sea. This northward moisture transport from Arabian Sea into
476 subtropical Indo-Pak sector enhances the high water vapor content and the convection
477 over the region as illustrated in Figs. 3a and 6b. Finally, it is interesting to observe that
478 both the R-SST and NE-SST simulations display northward moisture transport over
479 Arabian Sea, a feature, which is remarkably absent in the E-SST simulations, which show
480 an anomalous cyclonic cell over the Arabian Sea during 2010.

481 In other words, both the ENSO-related and intrinsic Indian Ocean SST variabilities may
482 have contributed to maintain the unusual moisture transport into the northwest Pakistan
483 and adjacent areas during the boreal summer of 2010.

484 **6. Conclusions and discussion**

485 The devastating floods over northwest Pakistan and adjacent north Indian region during
486 2010 summer monsoon had a severe impact on the society. Moreover, similar phenomena
487 were observed in 2011 and 2012. Various scientific aspects of these sub-tropical extreme
488 rainfall events were unraveled by previous studies such as their potential predictability,
489 the influence of southward intrusion of mid-latitude systems or westward shift of large-
490 scale circulation (Houze et al. 2011; Webster et al. 2011; Hong et al. 2011, Mujumdar et
491 al. 2012). Yet, the specific role of Indo-Pacific SST evolution in the occurrence of these
492 extreme events is unclear from the previous studies and is difficult to assess from
493 observations alone. In this study, the key-role of Indo-Pacific SST forcing in the

494 occurrence and intensity of sub-tropical Indo-Pak extreme rainfall episodes is explored
495 through different sets of sensitivity experiments with a very high resolution AGCM
496 forced by observed, ENSO and ENSO-unrelated SST anomalies during boreal spring and
497 summer of 2010.

498 Our first important result is that summer monsoon 2010 simulations using a very high-
499 resolution AGCM and observed SSTs could realistically capture the large-scale features
500 associated with these sub-tropical Indo-Pak extreme rainfall events, except the mid-
501 latitude atmospheric blocking. Furthermore, the more frequent occurrence of extreme
502 synoptic scale convective activity over northwest Pakistan region during 2010 is also well
503 captured by the simulations using observed SST boundary conditions, even though the
504 timing of these events is different in the simulations. Overall, these findings suggest that
505 the tropical Indo-Pacific SST anomalies are an important factor in determining the heavy
506 precipitation over northwest Pakistan and adjacent Indian region. These results are
507 surprising because AGCM experiments with prescribed SSTs over the Indian Ocean are
508 known to be subject to uncertainties related to inconsistency between latent heat flux and
509 SST over the warm pool regions that may lead to spurious atmospheric response
510 particularly during boreal summer (Wu and Kirtman 2004).

511 The realistic simulation of the background atmospheric state associated with 2010 Indo-
512 Pak extreme rainfall events, using real-time SST boundary conditions, motivated us to
513 explore the specific influence of ENSO and ENSO-unrelated SST variations through
514 additional atmospheric experiments. These unique sensitivity experiments use ENSO and
515 ENSO-unrelated SST boundary conditions derived from the inverse linear modeling
516 approach of Compo and Sardeshmukh (2010). As expected, the simulations using ENSO-

517 related SST anomalies during 2010 display a westward shift in the large-scale monsoon
518 circulation, a significant weakening of convection over the BoB and Central India and
519 anomalous southeasterly moisture transport into the northwest Pakistan region. However,
520 Indo-Pak heavy rainfall anomalies are poorly simulated in these experiments, suggesting
521 that the success of the R-SST simulations is not only due to ENSO forcing, but also due
522 to ENSO-unrelated SST variability during 2010.

523 Simulation experiments, carried out using ENSO-unrelated SST anomalies, exemplify the
524 suppression of convection over central and western equatorial Indian Ocean, through the
525 subsiding branch of enhanced convection over southeast Indian Ocean, and the
526 modulation of the large-scale monsoon circulation as key factors for enhancing the
527 northward moisture transport over Arabian Sea and northwest Pakistan regions during the
528 boreal summer of 2010. The enhanced convection over the southeast Indian Ocean seems
529 to be related to the growth of the negative IOD event peaking during the fall of 2010
530 (Hori et al. 2013). This ENSO-unrelated forcing also amplifies the weakening of
531 convective activities over BoB and thereby supports modulation of large-scale monsoon
532 circulation. Furthermore, the similarities between the NE-SST and NE-IO-SST sets of
533 experiments point specifically to the importance of the intrinsic Indian Ocean SST
534 variability in the occurrence of heavy rainfall events over northwest Pakistan during
535 2010. It is very surprising that the intense convective activity over northwest Indo-Pak
536 region at the daily time scale, represented here by mid-tropospheric vertical velocity, is
537 better simulated by ENSO-unrelated forcing as compared to that of ENSO forcing. Thus,
538 the ENSO forced westward shift of large-scale circulation over Indo-Pacific sector may
539 not be sufficient in promoting the sub-tropical Indo-Pak intense convective activity

540 during 2010.

541 However, a detailed analysis of the stream and potential functions of vertically integrated
542 moisture transport in various sets of simulations suggests that the success of R-SST
543 simulations in reproducing the high frequency of heavy rainfall events over northwest
544 Pakistan during the boreal summer of 2010 is due to the combined influence of ENSO
545 and ENSO-unrelated SST forcings. Both types of SST boundary forcing interact and play
546 a significant role in the buildup of high water vapor content in northwest Indo-Pak region
547 during 2010.

548 Overall, this study points to the key-role of intrinsic Indian Ocean SST anomalies in
549 inducing the northward moisture transport over Arabian Sea and sub-tropical Indo-Pak
550 region in the background of modulated large-scale Indo-Pacific summer monsoon
551 circulation by Pacific SST anomalies during 2010. Thus, our results highlight the
552 importance of a detailed monitoring of Indian Ocean variability and conditions, through
553 dedicated observation systems, for improving the accuracy of “extended-range”
554 prediction of future heavy rainfall events over South Asia, which are projected to be more
555 frequent in the future warming climate (Trenberth 2012; Menon et al. 2013).

556 It may be worth exploring how regional air-sea coupled interactions might have
557 modulated the background flow during 2010 boreal summer, an issue, which could not be
558 addressed in our forced modeling framework. This could be scope for future study using
559 coupled atmosphere-ocean models, which may give better insight into the complex air-
560 sea processes over the Indian Ocean, associated with heavy rainfall events. Finally, the
561 reasonable success of the LMDZ AGCM in reproducing the complex features of the

562 monsoon circulation during 2010 from the SST boundary forcing alone highlights that
563 such global climate model, with a telescopic zoom over a specific region, may be
564 successfully used to produce improved regional climate change projections world-wide
565 (based on CMIP5 simulations) in the framework of the ongoing Coordinated Regional
566 Downscaling Experiment (CORDEX South-Asia, <http://cccr.tropmet.res.in>).

567 **Acknowledgements:** The authors thank the Director of the Indian Institute of Tropical
568 Meteorology (IITM, Pune) for extending all support for this research work. IITM
569 receives full financial support from the Ministry of Earth Sciences (MoES), Government
570 of India. Pascal Terray is funded by Institut de Recherche pour le Développement (IRD,
571 France). Part of this work was done while Pascal Terray was a visiting scientist at IITM.
572 We finally acknowledge Ms. Josefine Ghattas and Dr. Sebastien Denvil for computational
573 support about using the LMDZ model.

574 **References:**

- 575 Behera, S., J. V. Ratnam, Y. Masumoto, T. Yamagata, 2013: Origin of extreme summers
576 in Europe: the Indo-Pacific connection. *Climate Dyn.*, **41**, 3-4, 663-676, DOI:
577 10.1007/s00382-012-1524-8.
- 578 Boschat, G., P. Terray, S. Masson, 2011: Interannual relationships between Indian summer
579 monsoon and Indo-Pacific coupled modes of variability during recent decades.
580 *Climate Dyn.*, **37**, 1019–1043, doi: 10.1007/s00382-010-0887-y.
- 581 Bowden, G. J., P. R. Barker, V. O. Shestopal, J. W. Twidell, 1983: The Weibull
582 distribution function and wind power statistics. *Wind Engineering*, *7*(2), 85-98.
- 583 Cadet, D., G. Reverdin, 1981: Water vapour transport over the Indian Ocean during
584 summer. *Tellus*, **33**, 476-486.
- 585 Chen, T. C., 1985: Global water vapor flux and maintenance during FGGE. *Mon. Wea.*
586 *Rev.*, **113**, 1801-1819.
- 587 Chou, C., C. A. Chen, P.H. Tan, K.T. Chen, 2012: Mechanisms for Global Warming
588 Impacts on Precipitation Frequency and Intensity. *J. Climate*. **25**, 3291–3306.
- 589 Compo, G., P. Sardeshmukh, 2010: Removing ENSO-related variations from the climate
590 records. *J. Climate*, **23**, 1957–6126, DOI: 10.1175/2009JCLI2735.1.
- 591 Conradsen, K., L.B. Nielsen, L.P. Prahm, 1984: Review of Weibull Statistics for
592 Estimation of Wind Speed Distributions. *J. Climate Appl. Meteor.*, **23**, 1173–1183.
- 593 Goswami, B.N., V. Venugopal, D. Sengupta, M. S. Madhusoodanan, and P. K. Xavier,

594 2006: Increasing trend of extreme rain events over India in a warming
595 environment, *Science* **314**, 1442-1445, Doi. 10.1126/science.1132027.

596 Halpert , M. S., C. F. Ropelewski, 1992: Surface temperature patterns associated with the
597 Southern Oscillation. *J. Climate*, **5**, 577-593.

598 Hong, C-C, H-H Hsu, N-H Lin, H. Chiu, 2011: Roles of European blocking and tropical-
599 extratropical interaction in the 2010 Pakistan flooding. *Geophys. Res. Lett.*, **38**,
600 L13806 doi:10.1029/2011GL047583.

601 Horii, T., I. Ueki, K. Ando, K. Mizuno 2013: Eastern Indian Ocean warming associated
602 with the negative Indian Ocean dipole: A case study of the 2010 event. *J.*
603 *Geophys. Res.*, **118**, doi:10.1002/jgrc.20071.

604 Hourdin, F., I. Musat , S. Bony, P. Braconnot , F. Codron, J-L. Dufresne, L. Fairhead, M-
605 A Filiberti, P. Friedlingstein, J-Y Grandpeix, G. Krinner, P. LeVan, Z-X Li, and F.
606 Lott 2006: The LMDZ4 general circulation model: climate performance and
607 sensitivity to parameterized physics with emphasis on tropical convection.
608 *Climate Dyn.*, **27**(7-8), 787-813, doi:10.1007/s00382-006-0158-0.

609 Houze, Jr. RA., K. L. Rasmussen, S. Medina, S. R. Brodzik, and U. Romatschke 2011:
610 Anomalous atmospheric events leading to the summer 2010 floods in Pakistan.
611 *Bull. Amer. Meteor. Soc.*, **92**, 291–298, doi:10.1175/2010BAMS3173.1.

612 Huffman, G. J., R. F. Adler, D. T. Bolvin, G. Gu, E. J. Nelkin, K. P. Bowman, Y. Hong ,
613 E. F. Stocker, and D. B. Wolff, 2007: The TRMM Multi-satellite Precipitation
614 Analysis: Quasi-Global, Multi-Year, Combined-Sensor Precipitation Estimates at

615 Fine Scale. *Journal of Hydrometeorology*, **8**, 38-55.

616 Justus, C. G., W. R. Hargraves, A. Mikhail, D. Graber, 1978: Methods for Estimating
617 Wind Speed Frequency Distributions. *J. Appl. Meteor.*, **17**, 350–353.

618 Kim, W. M., S. W. Yeh, J.H. Kim, J.S. Kug, M.H. Kwon, 2011: The unique 2009-2010 El
619 Nino event: A fast phase transition of warm pool El Nino to La Nina, *Geophys.*
620 *Res. Lett.*, **38**, L15809, doi: 10.1029/2011GL048521.

621 Kistler, R., Coauthors, 2001: The NCEP-NCAR 50 year reanalysis: monthly means CD-
622 Rom and documentation. *Bulletin of American Meteorological Society*, **82**, 247–
623 267.

624 Krishnan, R., 1998: Interannual variability of water vapor flux over the Indian summer
625 monsoon region as revealed from the NCEP/NCAR reanalysis (NNRA). WECRP-
626 104, WMO/TD-No.876, 340-343. First WCRP International Conference on
627 Reanalysis, Maryland, USA, 1997.

628 Kug, J-S., I-S Kang, 2006: Interactive feedback between the Indian Ocean and ENSO, *J.*
629 *Climate*, **19**, 1784–1801.

630 Lau, W. K., K. M. Kim, 2012: The 2010 Pakistan Flood and Russian Heat Wave:
631 Teleconnection of Hydrometeorologic Extremes. *Journal of Hydrometeorology*,
632 **13**, 392–403, doi: 10.1175/JHM-D-11-016.1.

633 Lindzen, R.S., S. Nigam, 1987: On the role of sea surface temperature gradients in
634 forcing low-level winds and convergence in the Tropics. *J. Atmos. Sci.*, **44**, 2418-

635 2436.

636 Luo, J-J., S. Wataru , Y. Masumoto, 2012: Indian Ocean warming modulates Pacific
637 climate change, *PNAS*, **109** (46): 18701–18706, doi: 10.1073/pnas.1210239109.

638 Mann, M. E., 2011: On long range dependence in global surface temperature series: An
639 editorial comment, *Climatic Change*, **107**, 267-276.

640 Martius, O, H. Sodemann, Joos, H. Pfahl S, A. Winschall, M. Croci-Maspoli, M. Graf, E.
641 Madonna, B. Mueller, S. Schemm, J. Sedláček, M. Sprenger, and H. Wernli,
642 2012: The role of upper-level dynamics and surface processes for the Pakistan
643 flood of July 2010. *Quart. J. Roy. Meteor. Soc.*, **139** (676), 1780-1797, DOI:
644 10.1002/qj.2082.

645 Menon, A., A. Levermann, J. Schewe, J. Lehmann, and K. Frieler, 2013: Consistent
646 increase in Indian monsoon rainfall and its variability across CMIP-5 models.
647 *Earth Syst. Dynam. Discuss.* **4**, 1–24.

648 Mujumdar, M., B. Preethi, T.P. Sabin, K. Ashok, S. Sajjad, D.S. Pai, and R. Krishnan,
649 2012: The Asian summer monsoon response to the La Niña event of 2010.
650 *Meteorological Applications* **19**, 216–225, DOI: 10.1002/met.1301.

651 Rasmussen, E. M., T. H. Carpenter, 1983: The relationship between eastern equatorial
652 Pacific SST and rainfall over India and Sri Lanka. *Mon. Wea. Rev.*, **111**, 517–528.

653 Rasmussen, K.L., A.J. Hill, V. E. Toma, M. D. Zuluaga, P. J. Webster, and R.A. Houze Jr.,
654 2014: Multiscale analysis of three consecutive years of anomalous flooding in
655 Pakistan, *Q.J.R. Meteorol. Soc.*, (under revision).

656 Rao, G. V., H.M.E. Van de Boogard, 1981: Structure of the Somali jet deduced from
657 Aerial observations taken during June-July 1977. Monsoon Dynamics. Ed.
658 R.P.Pearce and J. Lighthill, Cambridge Univerisity Press, 321-331.

659 Rayner, N., D. Parker, E. Horton, E. Folland, L. Alexander, d. Rowell, E. Kent, and A.
660 Kaplan, 2003: Global analyses of sea surface temperature, sea ice, and night
661 marine air temperature since the late nineteenth century. *Journal of Geophysical*
662 *Research*, **108**, 4407, doi:10.1029/ 2002JD002670.

663 Rousu, N.D., 1973:Weibull skewness and kurtosis as a function of the shape parameter.
664 *Technometrics*, **15** (4), 927-930.

665 Roxy, M. K., K. Ritika, P. Terray, S. Masson, 2014: The curious case of Indian Ocean
666 warming. *J.Climate*, **27**, 22, 8501-8509.

667 Saha, K. R., S. N. Bavedekar, 1973: Water vapour budget and precipitation over the
668 Arabian Sea during the northern summer. *Q.J.R. Meteorol. Soc.*, **99**, 273-287.

669 Sabin, T. P., R. Krishnan, J. Ghattas, S. Denvil, J-L. Dufresne, F. Hourdin, P. Terray,
670 2013: High resolution simulation of the South Asian monsoon using a variable
671 resolution global climate model, *Clim. Dynamics*, **41** (1), 173-194,
672 [doi:10.1007/s00382-012-1658-8](https://doi.org/10.1007/s00382-012-1658-8).

673 Sarkar, A., S. Singh, D. Mitra, 2011: Wind climate modeling using Weibull and extreme
674 value distribution. *International Journal of Engineering, Science and Technology*,
675 3(5), 100-106.

676 Terray, P., F. Chauvin, H. Douville, 2007: Impact of southeast Indian Ocean Sea Surface
677 Temperature anomalies on monsoon-ENSO-dipole variability in a coupled ocean-
678 atmosphere model. *Climate Dyn.*, **28**, 553-580, doi: [10.1007/s00382-006-0192-y](https://doi.org/10.1007/s00382-006-0192-y).

679 Trenberth, K. E., 2012: Framing the way to relate climate extremes to climate change.
680 *Climatic Change*, **115** (2), 283-290, doi: [10.1007/s10584-012-0441-5](https://doi.org/10.1007/s10584-012-0441-5).

681 Ullah, K., G. Shouting, 2013: A diagnostic study of convective environment leading to
682 heavy rainfall during the summer monsoon 2010 over Pakistan. *Atmospheric*
683 *Research*, **120-121**, 226–239.

684 Webster, P. J., V. E. Toma, H-M. Kim, 2011: Were the 2010 Pakistan floods predictable?
685 *Geophys. Res. Lett.*, **38**, L04806, doi:[10.1029/2010GL046346](https://doi.org/10.1029/2010GL046346).

686 Wu, R., B. Kirtman, 2004 : Understanding the impacts of the Indian Ocean on ENSO
687 variability in a coupled GCM. *J. Climate*, **17**, 4019–4031, doi:[10.1175/1520-0442\(2004\)017\4019:UTIOTI.2.0.CO;2](https://doi.org/10.1175/1520-0442(2004)017\4019:UTIOTI.2.0.CO;2).

688

689 Yang, J., Q. Liu, S-P. Xie, Z. Liu, L. Wu, 2007: Impact of the Indian Ocean SST basin
690 mode on the Asian summer monsoon. *Geophys. Res. Lett.*, **34**, L02708.
691 doi:[10.1029/2006GL028571](https://doi.org/10.1029/2006GL028571).

692 Yamagata, T., S.K. Behera, J-J. Luo, S. Masson, M. Jury, and S. A. Rao, 2004: Coupled

693 ocean-atmosphere variability in the tropical Indian Ocean, in Earth Climate: The
694 Ocean-Atmosphere Interaction, *Geophys. Monogr. Ser.*, **147**, 189–212, Edited by
695 C. Wang, S.-P. Xie and J. A. Carton, AGU, Washington, D. C.

696 **Table Caption:**

697 **Table 1:** Acronyms and SST boundary forcings for the different sets of LMDZ simulation
698 experiments.

Experiment	SST boundary condition
C-SST	Observed climatological SST
R-SST	Observed climatological SST + SST anomalies of 2010
E-SST	Observed climatological SST + ENSO related SST anomalies decomposed for 2010
NE-SST	Observed climatological SST + ENSO unrelated SST anomalies decomposed for 2010
NE-IO-SST	Observed climatological SST + ENSO unrelated SST anomalies over Indian Ocean decomposed for 2010

699 **Figure Captions:**

700 **Figure 1:** January to September monthly evolution of SST anomalies ($^{\circ}\text{C}$) and JJAS
701 seasonal mean SST anomalies during 2010 for (a) observed SST anomalies; (b) ENSO
702 component (c) ENSO-unrelated component. ENSO-related and ENSO-unrelated SST
703 patterns were estimated from monthly SST anomalies during 2010 following Compo and
704 Sardeshmukh (2010). SST anomalies are computed from the base period 1948-2010.
705 Monthly SSTs are taken from HadISST dataset (Rayner et al. 2003).

706 **Figure 2:** Spatial distribution of mean rainfall (shaded; unit: mm day^{-1}) superimposed on
707 mean vertically integrated moisture transport vectors (unit: $\text{Kg m}^{-1} \text{s}^{-1}$) for JJAS seasonal
708 average; for (a) TRMM rainfall climatology for the base period (1998 to 2010) and
709 moisture transport NCEP climatology (1950-2010); (b) ensemble mean of C-SST runs.
710 The moisture transport vectors are integrated from the surface pressure to the 300 hPa
711 level; (c) Differences of rainfall and moisture transport between C-SST simulated and
712 TRMM and NCEP climatologies (d) Histogram (black bars) of minimum daily mid-
713 tropospheric (500 hPa) vertical velocity time series extracted from the northwest Pakistan
714 region (70° – 74°E ; 30° – 36°N) during JJAS season in the C-SST experiments with fitted
715 Weibull Probability Density Function (PDF; black curve). The x-axis is 500-hPa vertical
716 velocity (unit: Pa/s), upward vertical velocity is negative. The y-axis is probability
717 density. The histogram is normalized by area (e.g. bin width by number of observations in
718 each bin) for better comparison with the fitted PDF. See text for further details.

719 **Figure 3:** Rainfall (shaded; unit: mm day^{-1}) and vertically integrated moisture transport
720 (unit: $\text{Kg m}^{-1} \text{s}^{-1}$) anomalies during boreal summer of 2010 for (a) TRMM rainfall

721 (shaded) and NCEP moisture transport (vector); (b) R-SST runs. For observations,
722 rainfall (vertically integrated moisture transport) anomalies are computed from the base
723 period 1998-2010 (1950-2010). The R-SST rainfall and vertically integrated moisture
724 transport anomalies are relative to the climatology estimated from the C-SST runs.

725 **Figure 4:** Fitted Weibull Probability Density Function (PDF) of minimum daily mid-
726 tropospheric (500 hPa) vertical velocity (unit: Pa/s) time series extracted from the
727 northwest Pakistan region (70° – 74° E; 30° – 36° N) during JJAS for the C-SST (black), R-
728 SST (blue), E-SST (red), NE-SST (green) and NE-IO-SST (purple) sets of experiments.
729 The inset shows the details of the left tail of the PDFs, which describes the occurrence of
730 extreme daily events in the simulations. The x-axis is 500 hPa vertical velocity, upward
731 vertical velocity is negative. The y-axis is probability density.

732 **Figure 5:** (a) North-south cross section of zonally averaged (60° – 75° E) meridional and
733 vertical wind anomalies over the west Indian Ocean (domain 20° S– 35° N) during JJAS of
734 2010 from NCEP; (b) same as (a), but for R-SST runs; (c) North-south cross section of
735 zonally averaged (85° – 110° E) meridional and vertical wind anomalies over the east
736 Indian Ocean (domain 20° S– 40° N) during JJAS of 2010 from NCEP; (d) same as (c), but
737 for R-SST runs; (e) East-west cross section of meridionally averaged (15° – 0) zonal and
738 vertical wind anomalies for the domain 30° – 240° E during JJAS of 2010 from NCEP; (f)
739 same as (e), but for R-SST runs. Upward vertical velocity is negative in all the panels.
740 The wind anomalies for the R-SST runs are relative to the climatology estimated from the
741 C-SST runs. NCEP wind anomalies are computed from the 1950-2010 climatology. East-
742 west circulation is plotted after removing the zonal mean from the circulation parameters.

743 **Figure 6:** Same as Figure 3, but for rainfall and vertically integrated moisture transport
744 anomalies during JJAS 2010 in (a) E-SST runs; (b) NE-SST runs; (c) NE-IO-SST runs,
745 respectively.

746 **Figure 7:** JJAS anomalies of potential function (unit: 10^7 Kg s^{-1}) and divergent
747 component of vertically integrated water vapor transport vector ($\text{Kg m}^{-1} \text{ s}^{-1}$) for (a) R-SST
748 runs; (b) E-SST runs and (c) NE-SST runs, respectively. Water vapor transport vectors are
749 vertically integrated from the surface to 300 hPa. The potential function and divergent
750 component of vertically integrated water vapor transport vectors are estimated on a global
751 domain, but are shown here only over the region of interest (Chen 1985; Krishnan 1998).
752 The anomalies are computed from the JJAS climatology of potential function and
753 divergent component of vertically integrated water vapor transport in the C-SST runs.
754 Anomalies significant at the 95% confidence level (using a Student two-tailed test) are
755 dotted.

756 **Figure 8:** (a) North-south cross section of zonally averaged ($60^\circ\text{--}75^\circ\text{E}$) meridional and
757 vertical wind anomalies over the west Indian Ocean (domain $20^\circ\text{S}\text{--}35^\circ\text{N}$) during JJAS of
758 2010 for NE-SST runs; (b) same as (a), but for E-SST runs; (c) East-west cross section of
759 meridionally averaged ($15^\circ\text{S}\text{--}0^\circ$) zonal and vertical wind anomalies for the domain 30°--
760 240°E during JJAS of 2010 for NE-SST runs; (d) same as (c), but for E-SST runs.
761 Upward vertical velocity is negative in all the panels. The wind anomalies for the NE-
762 SST and E-SST runs are relative to the climatology estimated from the C-SST runs.

763 **Figure 9:** JJAS anomalies of stream function (unit: 10^7 Kg s^{-1}) and rotational component
764 of vertically integrated water vapor transport vector ($\text{Kg m}^{-1} \text{ s}^{-1}$) for (a) R-SST runs; (b)

765 E-SST runs and (c) NE-SST runs, respectively. Anomalies significant at the 95%
766 confidence level (using a Student two-tailed test) are dotted.

Figure 1
[Click here to download Rendered Figure: Fig1.eps](#)

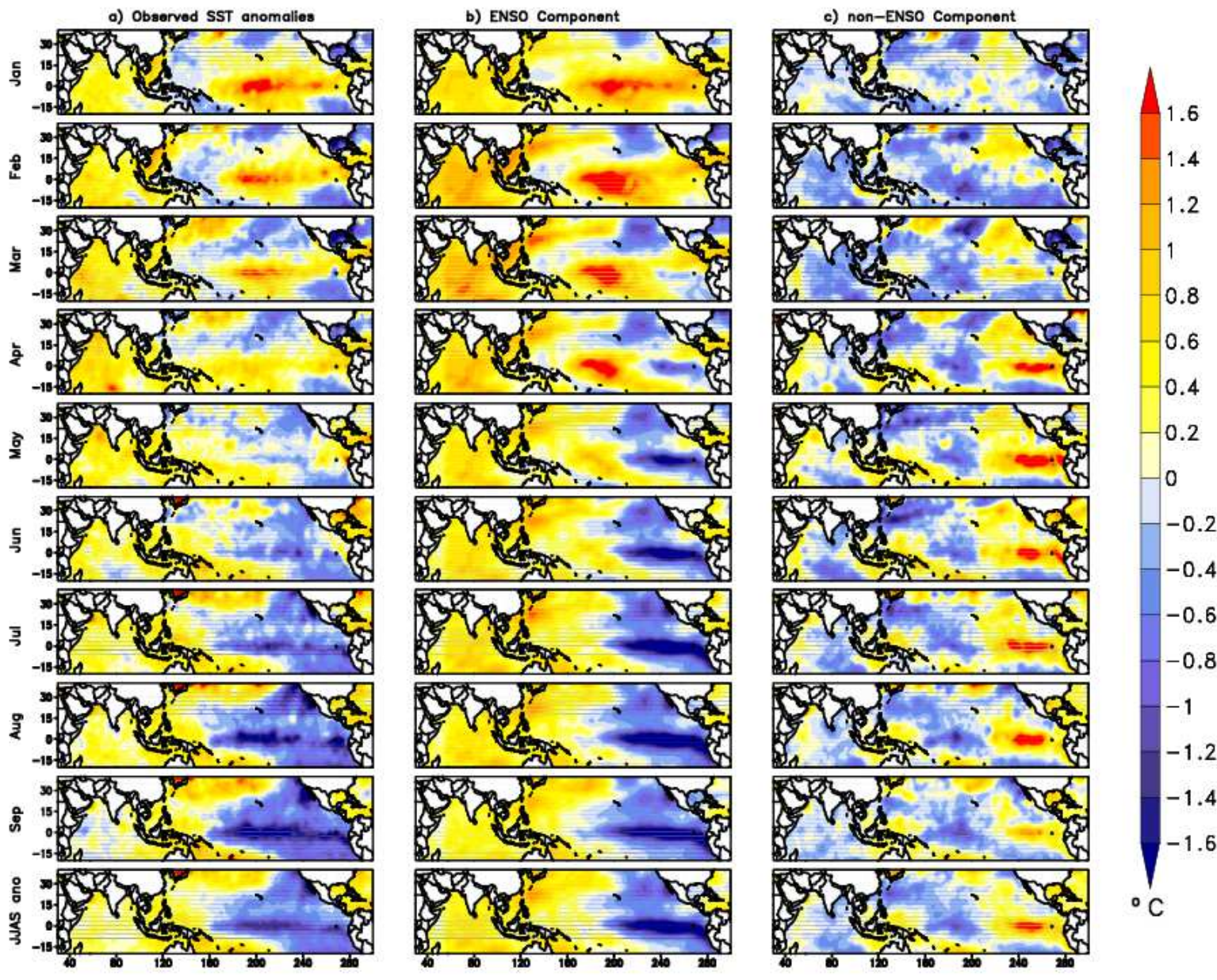


Figure 1: January to September monthly evolution of SST anomalies ($^{\circ}\text{C}$) and JJAS seasonal mean SST anomalies during 2010 for (a) observed SST anomalies; (b) ENSO component (c) ENSO-unrelated component. ENSO-related and ENSO-unrelated SST patterns were estimated from monthly SST anomalies during 2010 following Compo and Sardeshmukh (2010). SST anomalies are computed from the base period 1948-2010. Monthly SSTs are taken from HadISST dataset (Rayner et al. 2003).

Figure 2

[Click here to download Rendered Figure: Fig2.eps](#)

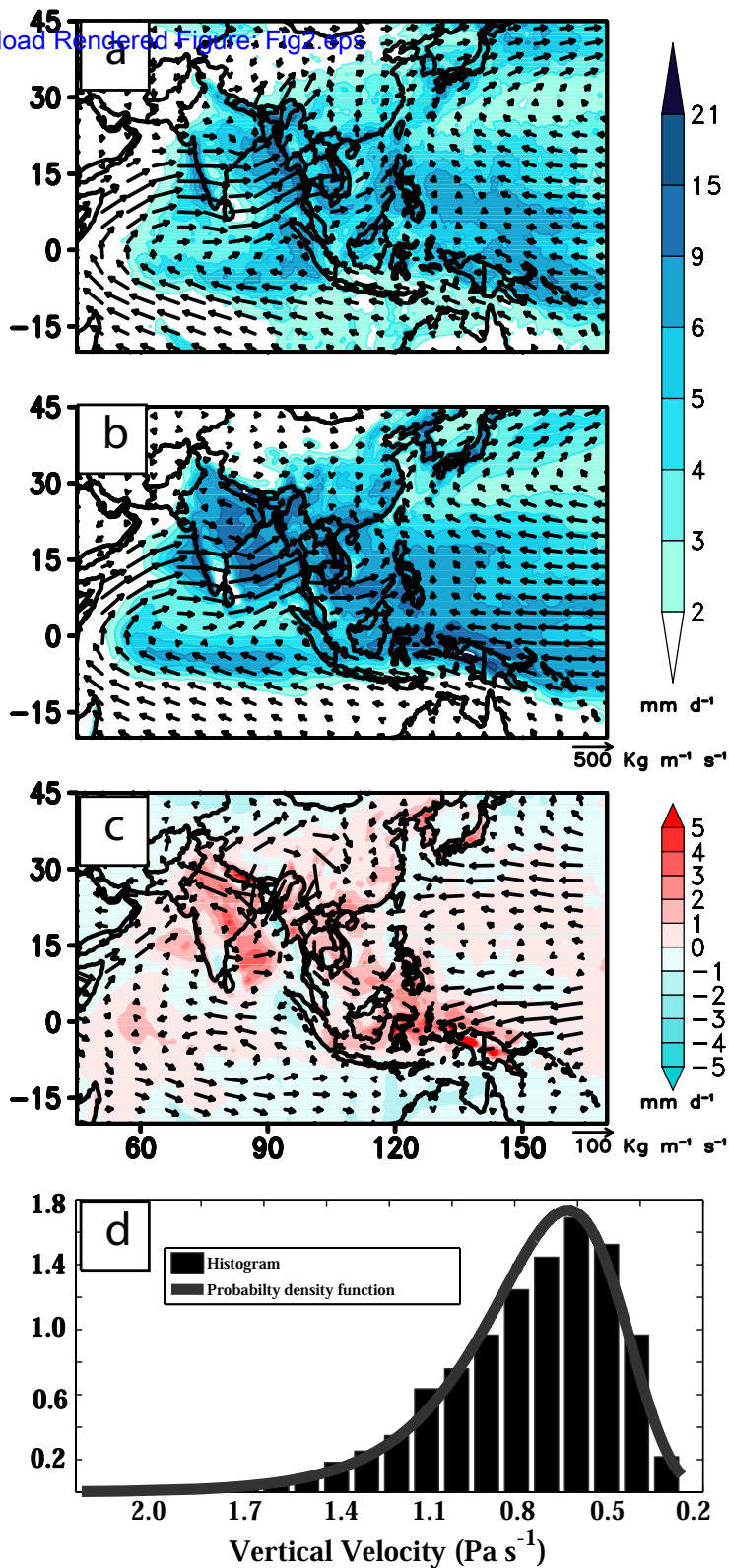


Figure 2: Spatial distribution of mean rainfall (shaded; unit: mm day^{-1}) superimposed on mean vertically integrated moisture transport vectors (unit: $\text{Kg m}^{-1} \text{s}^{-1}$) for JJAS seasonal average; for (a) TRMM rainfall climatology for the base period (1998 to 2010) and moisture transport NCEP climatology (1950-2010); (b) ensemble mean of C-SST runs. The moisture transport vectors are integrated from the surface pressure to the 300 hPa level; (c) Differences of rainfall and moisture transport between C-SST simulated and TRMM and NCEP climatologies (d) Histogram (black bars) of minimum daily mid-tropospheric (500 hPa) vertical velocity time series extracted from the northwest Pakistan region ($70^{\circ}\text{-}74^{\circ}\text{E}$; $30^{\circ}\text{-}36^{\circ}\text{N}$) during JJAS season in the C-SST experiments with fitted Weibull Probability Density Function (PDF; black curve). The x-axis is 500 hPa vertical velocity (unit: Pa/s), upward vertical velocity is negative. The y-axis is probability density. The histogram is normalized by area (e.g. bin width by number of observations in each bin) for better comparison with the fitted PDF. See text for further details

Figure 3
[Click here to download Rendered Figure: Fig3.eps](#)

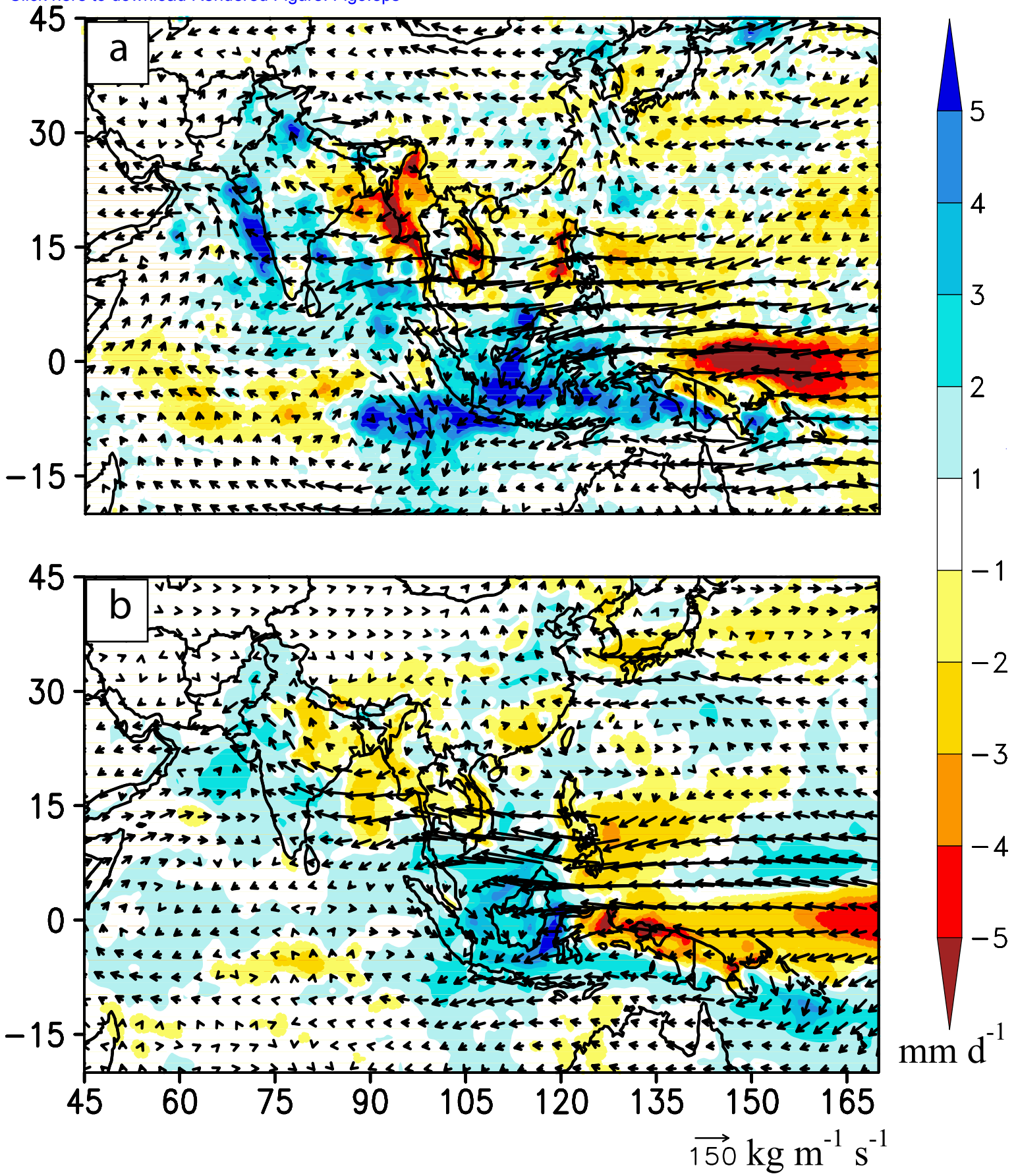


Figure 3: Rainfall (shaded; unit: mm day^{-1}) and vertically integrated moisture transport (unit: $\text{Kg m}^{-1} \text{ s}^{-1}$) anomalies during boreal summer of 2010 for (a) TRMM rainfall (shaded) and NCEP moisture transport (vector); (b) R-SST runs. For observations, rainfall (vertically integrated moisture transport) anomalies are computed from the base period 1998-2010 (1950-2010). The R-SST rainfall and vertically integrated moisture transport anomalies are relative to the climatology estimated from the C-SST runs.

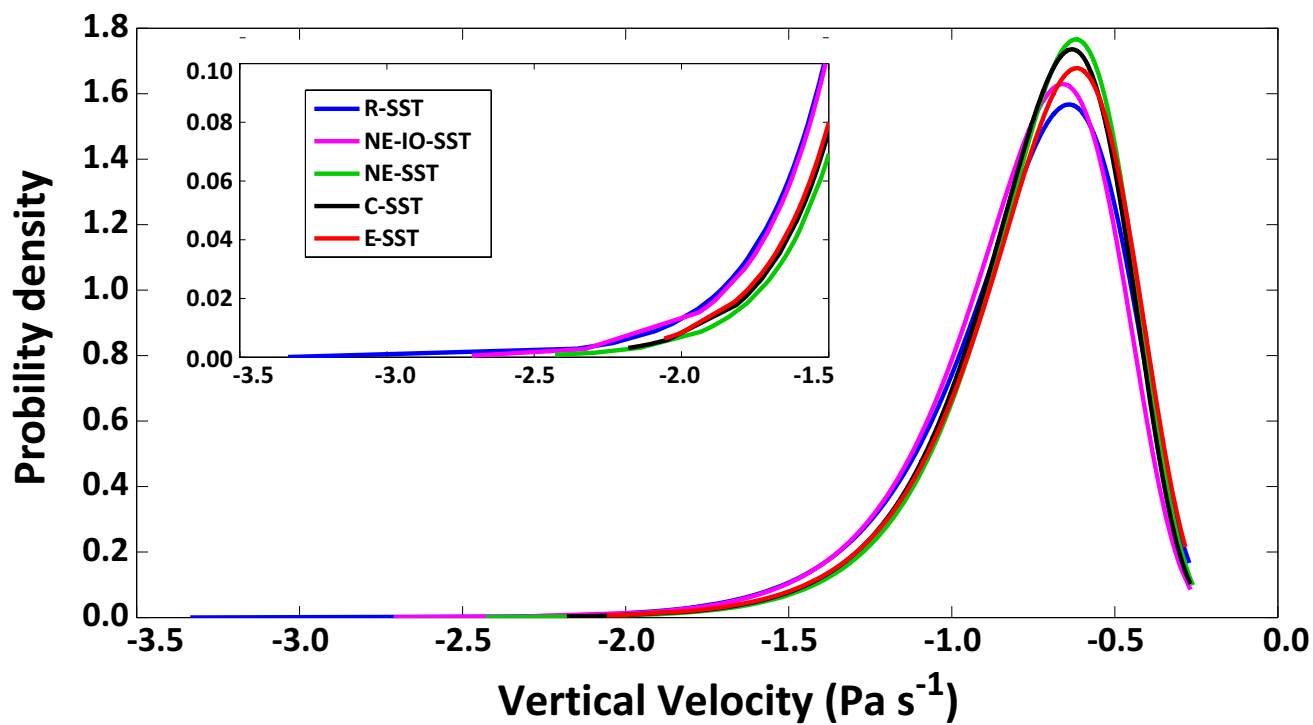


Figure 4: Fitted Weibull Probability Density Function (PDF) of minimum daily mid-tropospheric (500 hPa) vertical velocity (unit: Pa s⁻¹) time series extracted from the northwest Pakistan region (70°-74°E; 30°-36°N) during JJAS for the C-SST (black), R-SST (blue), E-SST (red), NE-SST (green) and NE-IO-SST (purple) sets of experiments. The inset shows the details of the left tail of the PDFs, which describes the occurrence of extreme daily events in the simulations. The x-axis is 500 hPa vertical velocity, upward vertical velocity is negative. The y-axis is probability density.

Figure 5
[Click here to download Rendered Figure: Fig5.eps](#)

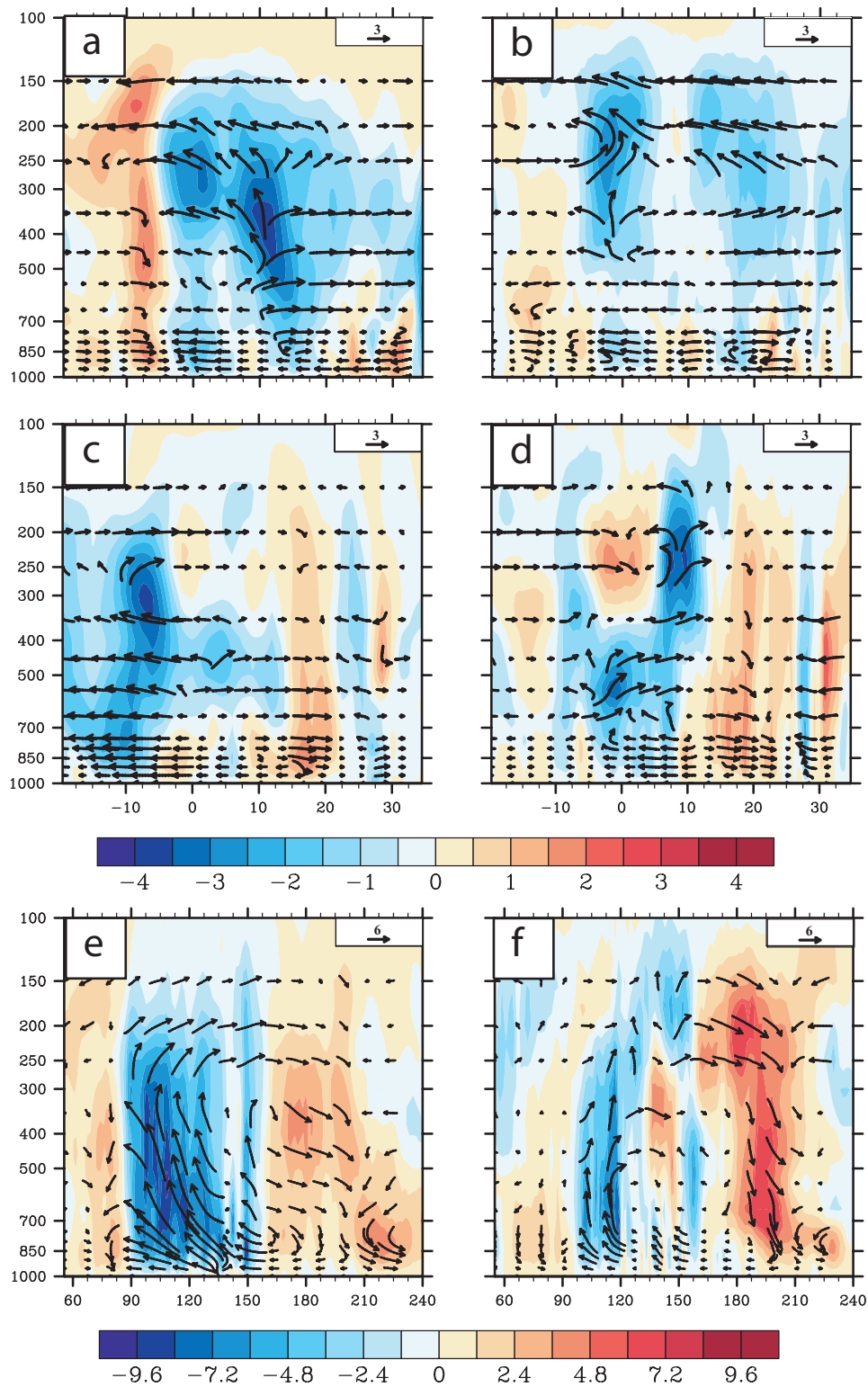


Figure 5: (a) North-south cross section of zonally averaged (60° - 75° E) meridional and vertical wind anomalies over the west Indian Ocean (domain 20° S- 35° N) during JJAS of 2010 from NCEP; (b) same as (a), but for R-SST runs; (c) North-south cross section of zonally averaged (85° - 110° E) meridional and vertical wind anomalies over the east Indian Ocean (domain 20° S- 40° N) during JJAS of 2010 from NCEP; (d) same as (c), but for R-SST runs; (e) East-west cross section of meridionally averaged (15° - 0°) zonal and vertical wind anomalies for the domain 30° - 240° E during JJAS of 2010 from NCEP; (f) same as (e), but for R-SST runs. Upward vertical velocity is negative in all the panels. The wind anomalies for the R-SST runs are relative to the climatology estimated from the C-SST runs. NCEP wind anomalies are computed from the 1950-2010 climatology. East-west circulation is plotted after removing the zonal mean from the circulation parameters.

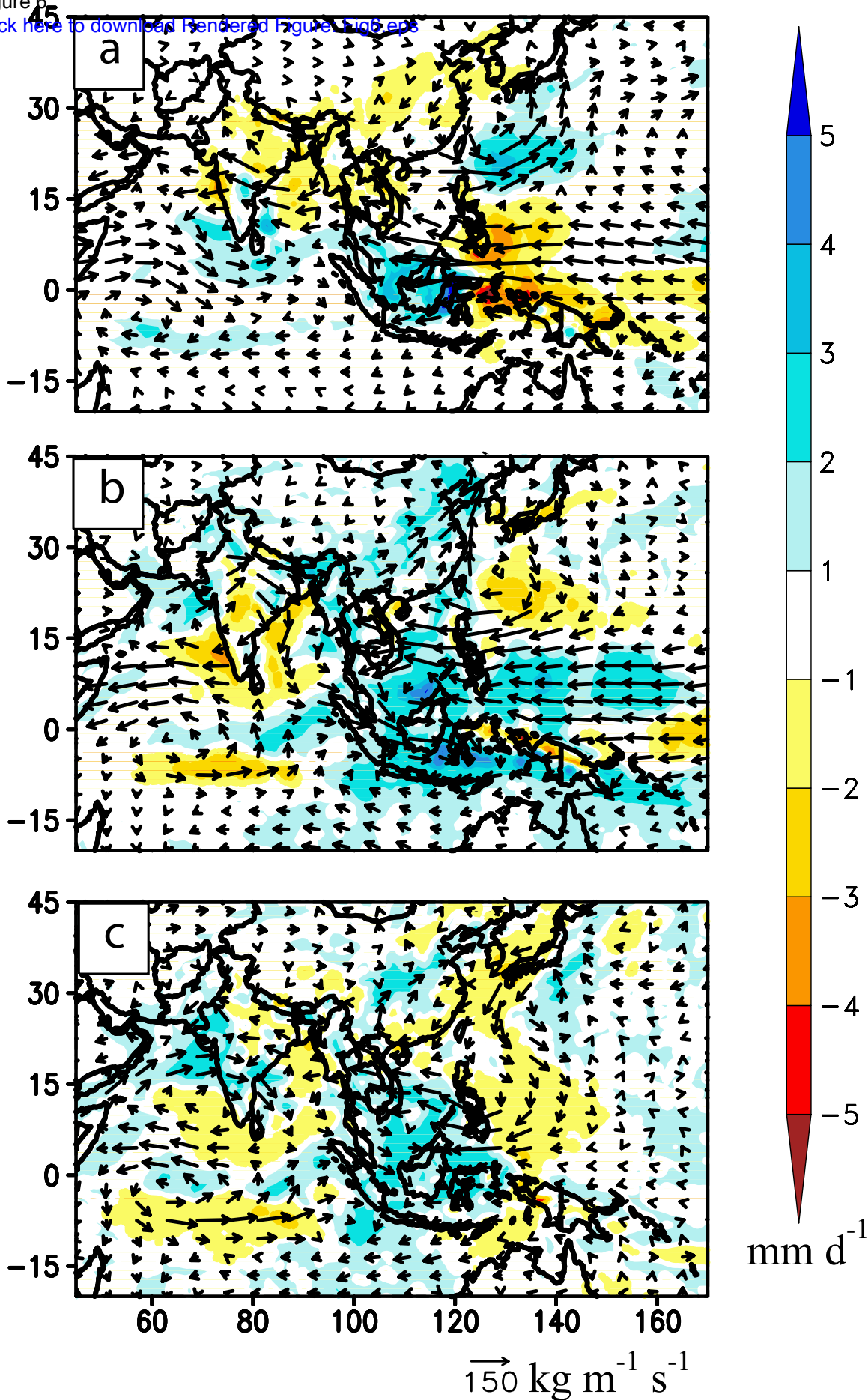


Figure 6: Same as Figure 3, but for rainfall and vertically integrated moisture transport anomalies during JJAS 2010 in (a) E-SST runs; (b) NE-SST runs; (c) NE-IO-SST runs, respectively.

Figure 7

[Click here to download Rendered Figure: Fig7.eps](#)

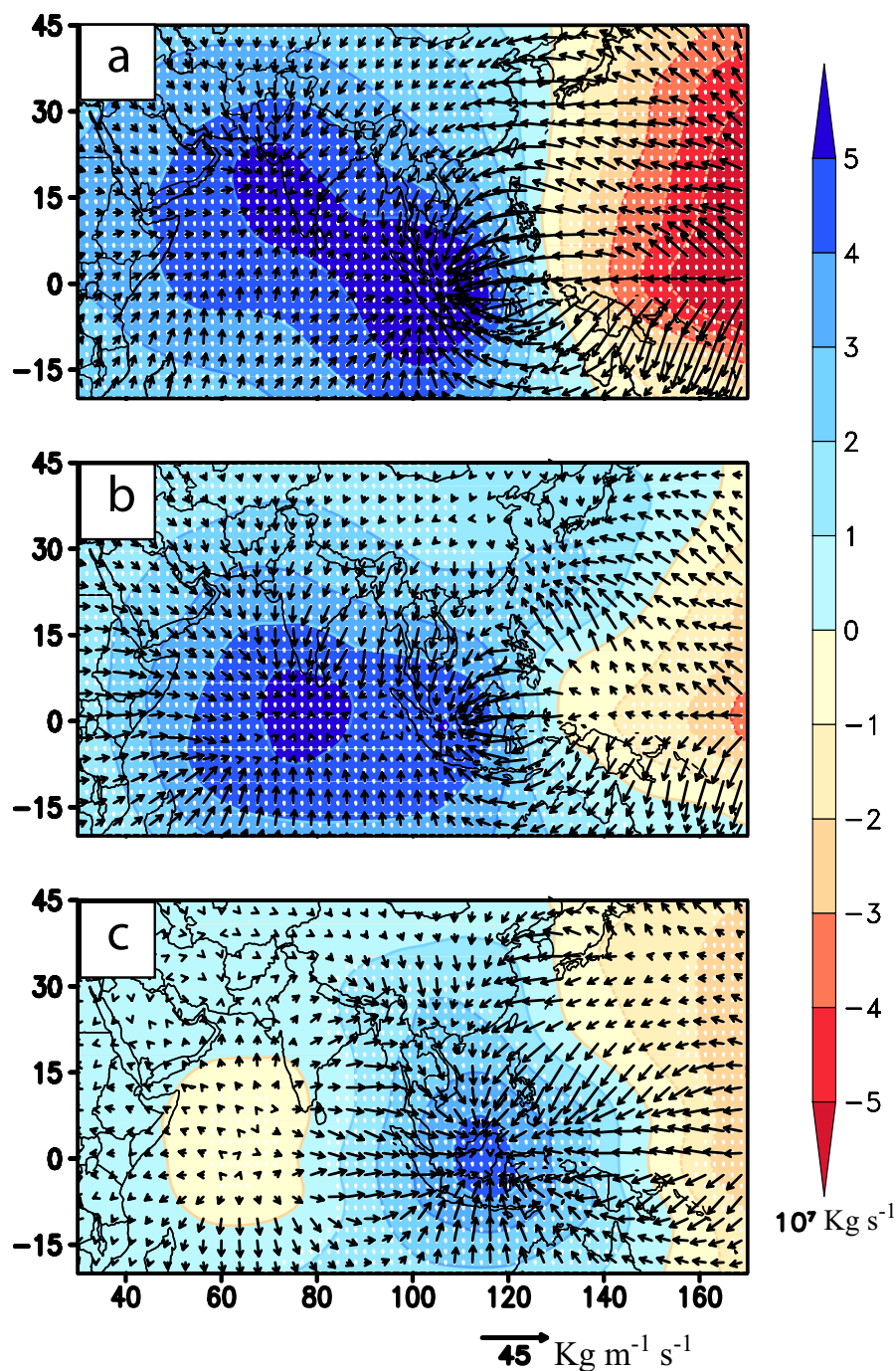


Figure 7: JJAS anomalies of potential function (unit: 10^7 Kg s^{-1}) and divergent component of vertically integrated water vapor transport vector ($\text{Kg m}^{-1} \text{ s}^{-1}$) for (a) R-SST runs; (b) E-SST runs and (c) NE-SST runs, respectively. Water vapor transport vectors are vertically integrated from the surface to 300 hPa. The potential function and divergent component of vertically integrated water vapor transport vectors are estimated on a global domain, but are shown here only over the region of interest (Chen 1985; Krishnan 1998). The anomalies are computed from the JJAS climatology of potential function and divergent component of vertically integrated water vapor transport in the C-SST runs. Anomalies significant at the 95% confidence level (using a Student two-tailed test) are dotted.

Figure 8
[Click here to download Rendered Figure: Fig8.eps](#)

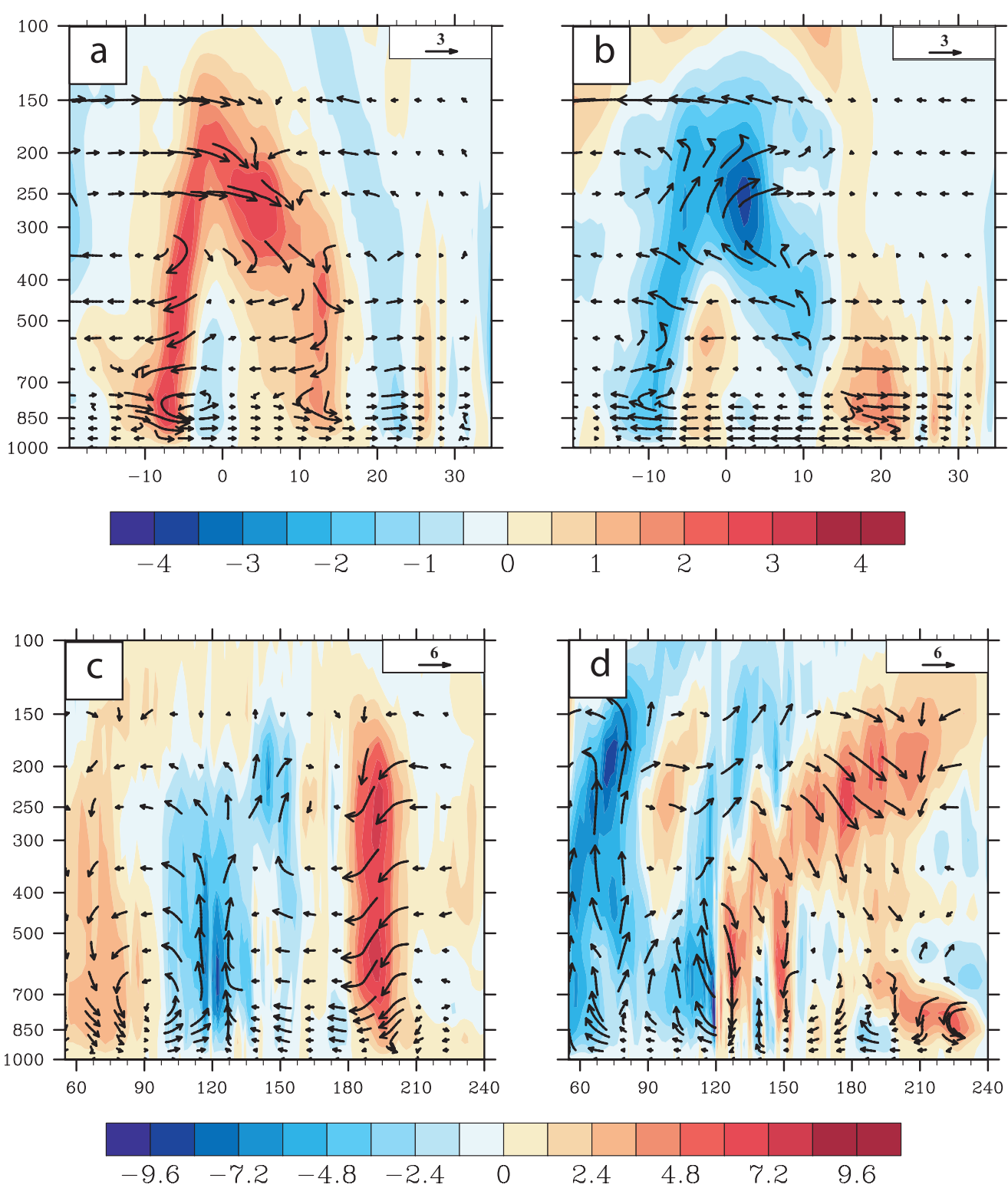


Figure 8: (a) North-south cross section of zonally averaged (60° - 75° E) meridional and vertical wind anomalies over the west Indian Ocean (domain 20° S- 35° N) during JJAS of 2010 for NE-SST runs; (b) same as (a), but for E-SST runs; (c) East-west cross section of meridionally averaged (15° S- 0°) zonal and vertical wind anomalies for the domain 30° - 240° E during JJAS of 2010 for NE-SST runs; (d) same as (c), but for E-SST runs. Upward vertical velocity is negative in all the panels. The wind anomalies for the NE-SST and E-SST runs are relative to the climatology estimated from the C-SST runs.

Figure 9

[Click here to download Rendered Figure: Fig9.eps](#)

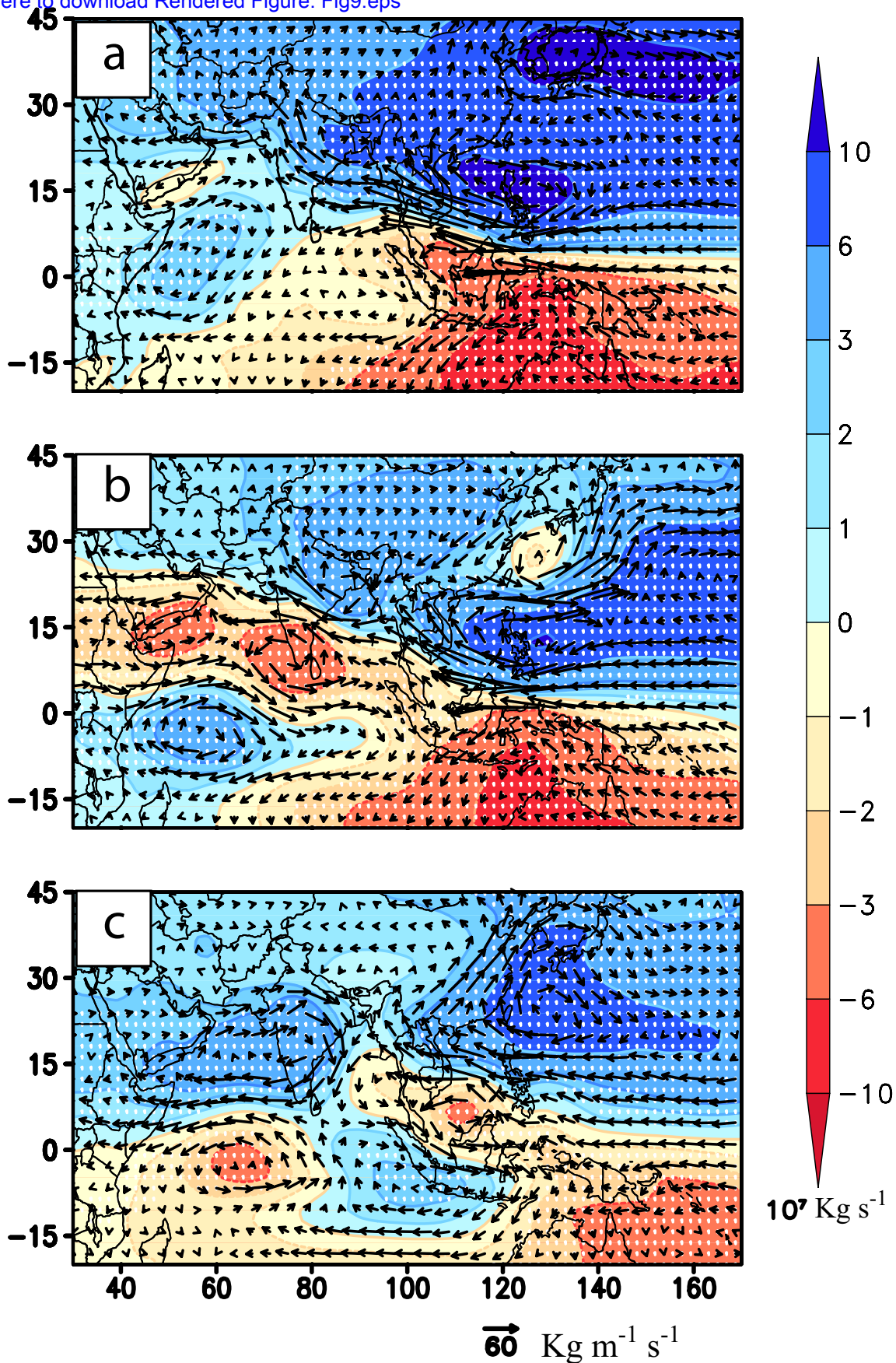


Figure 9: JJAS anomalies of stream function (unit: 10^7 Kg s^{-1}) and rotational component of vertically integrated water vapor transport vector ($\text{Kg m}^{-1} \text{ s}^{-1}$) for (a) R-SST runs; (b) E-SST runs and (c) NE-SST runs, respectively. Anomalies significant at the 95% confidence level (using a Student two-tailed test) are dotted.

Experiment	SST boundary condition
C-SST	Observed climatological SST
R-SST	Observed climatological SST + SST anomalies of 2010
E-SST	Observed climatological SST + ENSO related SST anomalies decomposed for 2010
NE-SST	Observed climatological SST + ENSO unrelated SST anomalies decomposed for 2010
NE-IO-SST	Observed climatological SST + ENSO unrelated SST anomalies over Indian Ocean decomposed for 2010

Table 1: Acronyms and SST boundary forcings for the different sets of LMDZ simulation experiments.